Design of an LQR Control Strategy for Implementation on a Vehicular Active Suspension System

Ben Creed, Nalaka Kahawatte, Scott Varnhagen
MAE 272 – winter 2010 – Paper II
University of California, Davis

1. Introduction

This paper discusses the implementation of a Linear Quadratic Regulator (LQR) optimal controller for an active suspension system on a standard mid size sedan. A detailed analysis of the construction and verification of the vehicle model is included. The goal of the LQR controller is to improve passenger ride comfort by minimizing the effect of external disturbances felt by the passenger such as road irregularities, cornering and braking. This is accomplished by actively applying vertical forces in the suspension. As a result, these systems can be used to minimize vehicle body roll, vertical accelerations experienced by the passengers, and improve overall vehicle handling.

Such systems are becoming increasingly common on both passenger and commercial vehicles. For example, the active suspension system developed by Bose Corporation is utilized in many of the luxury sedans in today's market.[1]

2. System Description

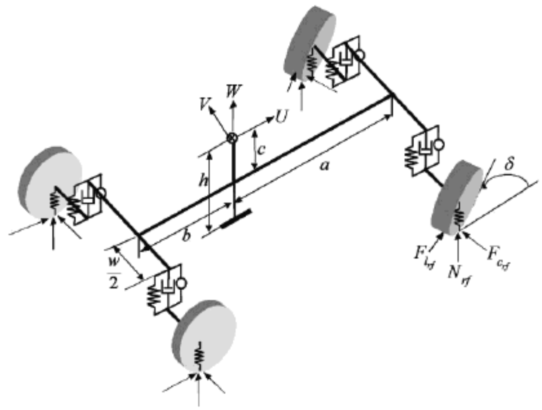

Figure 1.1: Full Car Model with suspension units [2]

The vehicle model includes a suspension unit at each corner of the vehicle which consists of a spring, damper and a force actuator as shown in Figure 1.1. The constitutive behavior of these elements are non-linear and the linearization process is discussed in section 3.2.

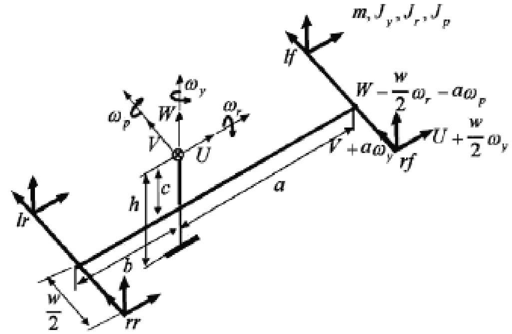

Figure 1.2: Coordinate System for the rigid body[1]

The vehicle chassis is modeled as a rigid body with body fixed coordinates, U,V,W attached at the Center of Gravity (CG) and aligned in its principal directions as shown in Figure 1.2. The body has mass, m, and moments of inertia J_r (roll) about the U-axis, J_p (pitch) about the V-axis, and J_y (yaw) about the W-axis. The CG is located a distance 'a' from the front axle, 'b' from the rear axle, and 'h' from the ground. The half-width of the vehicle is w/2.

The suspension actuators are implemented simply as controllable force inputs. The physical method of force actuation is not discussed in this paper. This will allow more flexibility once the control system has been designed for selecting the most appropriate actuator. The force actuation can be accomplished using a variety of components. Some examples include electromechanical actuators, hydraulic actuators, and pneumatic actuators. Each system has its own distinct strengths such as response time and power requirements.

2.1 Parameter Definition

2.1.1 Physical Parameters

Table 2.1: Physical Parameters

Variable	Parameter
δ	Steering Angle (rad)
a	Distance from CG to Front Axle (m)
b	Distance from CG to Rear Axle (m)
b_{sF}	Damper Coefficient – Front (N-s/m)
b_{sR}	Damper Coefficient – Rear (N-s/m)
F_{brake}	Total Braking Force (N)
F_{pitch}	Pitching Force on CG (N)
F_{roll}	Rolling Force on CG (N)
F_{FR}	Controlled Actuator Output Front Right (N)
F_{FL}	Controlled Actuator Output Front Left (N)
F_{RR}	Controlled Actuator Output Rear Right (N)
F_{RL}	Controlled Actuator Output Rear Left (N)
h	Height of CG from Road (m)
J_p	Pitch Moment of Inertia (kg/m^2)
J_r	Roll Moment of Inertia (kg/m^2)
k_t	Tire Stiffness (N/m)
k_s	Spring Stiffness (N/m)
m_s	Mass of Vehicle (kg)
m_{us}	Unsprung Mass (kg)
U	Forward Velocity (m/s)
$V_{CG(t)}$	Vertical Velocity of CG (m/s)
$V_{FR(t)}$	Velocity Input Front Right (m/s)
$V_{FL(t)}$	Velocity Input Front Left (m/s)
$V_{RR(t)}$	Velocity Input Rear Right (m/s)
$V_{RL(t)}$	Velocity Input Rear Left (m/s)
w	Track Width (m)

2.1.2 State Variables Definition

Table 2.2: State Variable Definitions

Variable	Parameter
L_R	Roll Angular Momentum (N.m.s)
L_P	Pitch Angular Momentum (N.m.s)
p_{usRR}	Unsprung Momentum Rear Right (kg.m/s)
p_{usRL}	Unsprung Momentum Rear Left (kg.m/s)
p_{usFR}	Unsprung Momentum Front Right (kg.m/s)
p_{usFL}	Unsprung Momentum Front Left (kg.m/s)
p_{VCG}	Vertical Momentum of CG (kg.m.s)
x_{TRR}	Tire Deflection Rear Right (m)
x_{TRL}	Tire Deflection Rear Left (m)
x_{TFR}	Tire Deflection Front Right (m)
x_{TFL}	Tire Deflection Front left (m)
x_{SRR}	Spring Deflection Rear Right (m)
x_{SRL}	Spring Deflection Rear Left (m)
x_{SFR}	Spring Deflection Front Right(m)
x_{SFR}	Spring Deflection Front Left (m)

2.2 Inputs

The system has ten inputs, six of which are exogenous and the others controllable. These inputs are:

Exogenous:

- The road velocity inputs experienced at each wheel
- Vehicle pitch force (due to accelerating/braking/cornering the vehicle)
- Vehicle roll input (due to cornering the vehicle)

Controllable:

- Actuator forces applied to the suspension system at each corner of the vehicle

In this simulation, the road inputs, vehicle pitch, and roll will be simulated based on three different driving scenarios:

1. Driving over a "speed bump" by generating a vertical velocity profile input
2. Braking at 1 g by applying the appropriate pitch moment to the vehicle center of gravity
3. Cornering by applying the appropriate pitch and roll moment to the vehicle center of gravity

2.3. Outputs

The model used in this simulation is composed of 15 separate state variables, however not all of these states are relevant to the control of an active suspension system.

The ride quality can be quantified by examining the vertical and angular accelerations of the vehicle body, as well as the ability for the vehicle to remain level regardless of operating conditions. [7]

The 15 states in this model each correspond to the state of an energy storing element. The following states are observed using the C matrix:

- The deflection of the suspension springs
- The deflection of the tire springs
- The vertical and angular velocities of the vehicle's center of gravity

3. System Model

3.1.1. Modeling Methodology

Modeling the aforementioned system began with the creation of a 'bond graph' of the system. Bond graphs are a concise pictorial representation of all types of interacting energy domains, and are an excellent tool for representing vehicle dynamics with associated control hardware[1]. Each bond represents a pair of signals (effort and flow) whose product is the instantaneous power of the bond. In the case of a mechanical system, effort and flow translate into force and velocity respectively. The 'half arrow' sign convention defines the direction of energy flow. The energy storing elements in the bond graph define the number of state variables in the system and using the established methods in bond graphing, state equations can be derived directly from the bond graph [4].

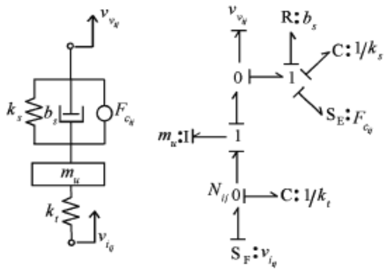

Figure 1.1: Schematic of a single suspension unit and the corresponding bond graph [1]

For illustration purpose, the schematic and the corresponding bond graph for a single suspension unit is shown in Figure 3.1. Please refer to Appendix A for the complete bond graph of the system.

The set of state equations were derived using the complete bond graph as further discussed in section 3.3. State-space matrices (A,B,C,D) were derived using these system equations and are discussed further in section 3.4.

3.1.2. Underlying Assumptions

The objective of the model created was to assist in the development of a control system for the vehicle's active suspension system. A high level of detail could have been included in the development of the model, however assumptions were made to simplify the model. These simplifications help remove unnecessary details that are not of interest when optimizing the vertical dynamics of the vehicle. The assumptions also help reduce the computational requirements of the simulation.

The following assumptions were made to simplify the model:

- The body of the vehicle is rigid.
- The lateral and longitudinal motion of the tires is negligible compared to their vertical motion.
- The vehicle is a neutral steer car[1,2]
- The vehicle is not skidding

Because lateral and longitudinal dynamics have been removed from the model, it was important to approximate their effects on the vertical behavior of the model during braking/cornering. The approximated braking/cornering forces are applied to the CG of the vehicle, as discussed in more detail in the Simulation section of the paper (Section 4.3-4.4).

3.2 Linearization

A strength of bond graph modeling is the ability to use a single model for both linear and nonlinear systems over multiple energy domains. The ordinary differential equations that describe the system are extracted directly from the bond graph using a straightforward procedure. Each component has particular constitutive laws that describe its behavior and are tied together at the time of equation formulation. The switch from a nonlinear to a linear component comes from a simple substitution in the bond graph equations.

The modeled components are in reality nonlinear; however a standard linearization process can be executed for each component. Figure 4.1 shows a hypothetical tire deflection curve in red and its linearization.

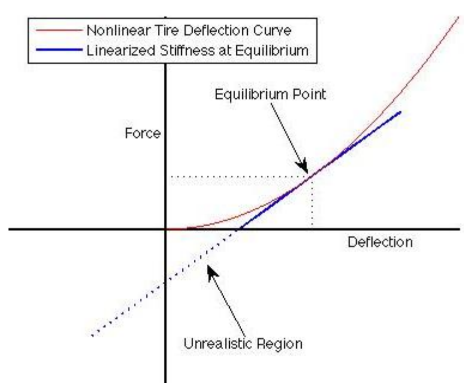

Figure 4.1: Tire Deflection Curve and Linearization

A tire is unable to "pull" (provide negative force) since it is not attached to the ground. In addition, the positive force that it supplies is nonlinear. To linearize this tire, the equilibrium point on the actual curve must be located. For small deviations from the equilibrium point, the constitutive behavior of the spring may be considered linear as shown in blue. The linear tire is a particularly complicated component due to its inability to prevent the application of negative force. This must be dealt with by adding logic into the simulation code, or by scaling the inputs to prevent tire lift-off.

The suspension springs, and dampers would typically undergo a similar linearization process. This particular model however is based loosely on actual vehicle data of a mid size sedan as mentioned in reference [1], and the original equations that were linearized to provide the constants tabulated in table 1 were unavailable.[1]

The following assumptions about linearity were made in our model:

- Each tire is modeled as a single linear spring
- Each of the suspension springs are linear
- Every linear spring element (tire and suspension) has an equilibrium displacement calculated by the static vehicle model sitting in a gravity acceleration field
- Each of the suspension dampers are linear
- Each of the active suspension force actuators are linear

The linearity of this model permits the use of a state-space representation of the system. This results in first-order explicit differential equations of the form shown in Equation 4.1 that are easily numerically integrated.

$$\dot{X} = AX + BU \qquad (4.1)$$

3.3 State Variables & Linearized System Equations

As discussed previously in section 3.1, using the bond graph, 15 state variables were identified and linear state equations were obtained. Please refer to Appendix B for the complete set of state equations. For more information on the procedure of deriving state equations using bond graphs, please refer to reference [4].

3.4 State-Space Representation

Please refer to Appendix C for the complete set of state space representation matrices obtained from the linearized state equations.

4. Simulation

Table 4.1 shows the linear parameters used for the vehicle simulation, which are loosely based on a standard sedan [1]. These parameters were used to populate the state-space representation of the model shown in Appendix C. A Simulink model was constructed which allowed inputs and outputs to be applied to/recorded from a state-space block. The Simulink block diagram and the state-space A,B,C,D matrix population code can be viewed in Appendix D and G respectively.

Table 4.1: Parameter Values for Simulation

Parameter	Value
Vehicle	
Distance from Cg to front axle (a)	1.17m
Distance from Cg to rear axle (b)	1.68m
Height of Cg above the road (h)	0.55m
Track (w)	1.54m
Mass of the car (m_s)	1513 kg
Roll moment of inertia (J_r)	637.26 kgm^2
Pitch moment of inertia (J_p)	2443.26 kgm^2
Anti-roll bar stiffness (k_a)	1.5 x 10^6 N/m
Tire	
Unsprung mass (m_{us})	38.42 kg
Tire stiffness (k_t)	150,000 N/m
Suspension	
Suspension stiffness (k_s)	14,900 N/m
Damper coefficients (b_s)	475 Ns/m

4.1 Model Validation using a quarter-car

Before complicated full car simulations could be conducted, it was necessary to ensure that basic properties indicative of the quarter car model were evident in the simulation results. To simulate the model as a quarter car, the model was made geometrically symmetric by setting distance "a" equal to distance "b", effectively placing the model's center of gravity symmetrically between the front and rear of the vehicle. By inputting the same velocity at each corner of the vehicle, the body of the vehicle exhibited only vertical motion, represented by a simple mass-spring-damper system, as shown below in Figure 4.1.

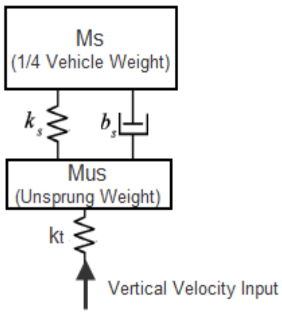

Figure 4.1: Quarter Car Model

Analysis of this simple spring-mass-damper system produced Equation 4.1 and 4.2 which, when evaluated with the parameters listed in Table 4.1, resulted in a body natural frequency of 0.95Hz, and a wheel natural frequency of 10.4Hz. [4]

$$\mathbf{f_{body}} = \left(\frac{\mathbf{1}}{\mathbf{2\pi}}\right)\sqrt{\frac{\mathbf{ks*kt}}{\mathbf{(ks+k_t)*m_{b/4}}}} = \mathbf{0.95Hz} \tag{4.1}$$

$$\mathrm{f_{wheel}} = \left(\frac{1}{2\pi}\right)\sqrt{\frac{\mathrm{ks+kt}}{\mathrm{m_{us}}}} = 10.4\ \mathrm{Hz} \tag{4.2}$$

The vehicle model was given a velocity step input of 5 m/s at each corner, lasting for 0.2 seconds. The abrupt application of velocity excited the faster wheel hop frequency, which was quickly damped giving way to the slower body oscillations as seen below in Figure 4.2. A Fast Fourier Transform was applied to the resulting suspension displacement data, and the dominant frequency was found to be 0.95Hz which correlates with the anticipated value calculated in Equation 4.1.

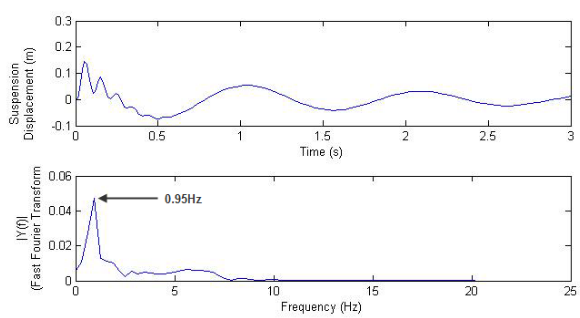

Figure 4.2: Body Natural Frequency FFT

To focus on recording the wheel natural frequency, the Fast Fourier Transform was concentrated on the first quarter second of the simulation when fast oscillations were prevalent. The result, shown below in Figure 4.3 is in agreement with the frequency predicted by Equation 4.2. The full vehicle model behaved as expected when simulated as a quarter car.

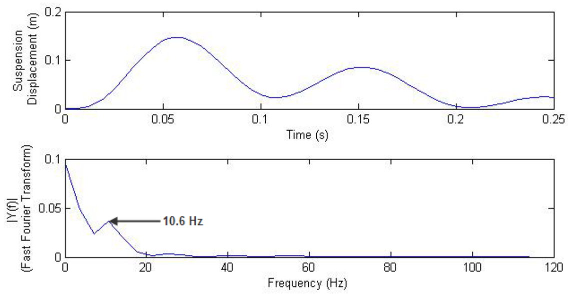

Figure 4.3: Wheel Hop natural Frequency FFT

4.2 Scenario 1 – Road Irregularity

To evaluate the vehicle's performance over road irregularities, a triangular profile speed bump was constructed with a width of 20cm, and a height of 5cm. The vehicle was simulated driving over the bump at 5m/s (18 km/h), producing the tire displacement plot shown In Figure 4.4. The front of the vehicle encounters the bump first, with the rear of the vehicle shortly following.

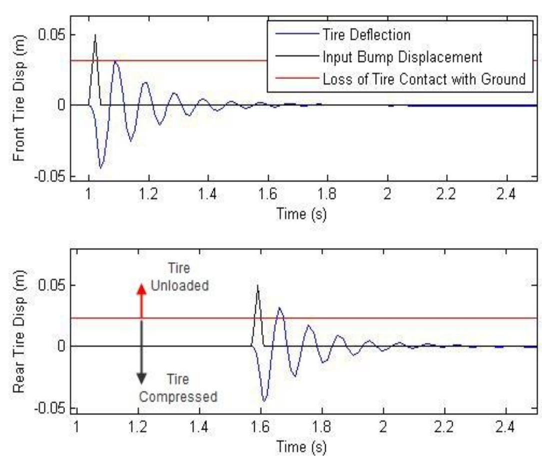

Figure 4.4: Tire Displacement Driving Over Speed-Bump at 5m/s

As described in the Section 3.2, the linearized tire may produce force in both compression and tension, while a true tire may only produce force while compressed. Driving over a bump too quickly with a physical vehicle will cause the tires to leave the ground momentarily at the exit of the bump. Figure 4.4 shows the displacement of the front and rear tires of the vehicle from equilibrium. As it can be observed, the front tires of the vehicle remain in contact with the ground. Unfortunately, the rear tires of the vehicle lift off the ground shortly after encountering the bump. This behavior must be detected and avoided as the linear tire model used here does not account for such situations.

4.3 Scenario 2 - Braking

To understand how the uncontrolled model reacted to braking, a step input equivalent to the force of braking at 1.0 g (calculated using Equation 4.3) was applied to the pitch axis of the vehicle.

$$F_{brake} = (m_{us} + m_{us}) * a \qquad (4.3)$$

$$F_{brake} = (1513kg + 4 * 38.42kg) * \frac{9.81m}{s^2} = 16350N$$

The resulting pitch angle, and angular acceleration of the vehicle about its center of gravity are show below in Figure 4.5. During the transient period following the application of the force, the vehicle experiences oscillating angular accelerations about the pitch axis which would be uncomfortable to the occupants of the vehicle.

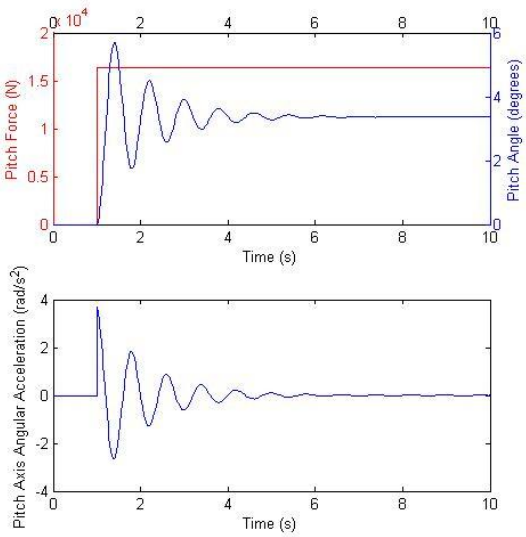

Figure 4.5: 1.0 g Braking

These oscillations are likely exaggerated due to the instantaneous nature of a step input, and would likely be reduced during a physical braking test. These oscillations are mostly damped out of the system within 5 seconds, and the vehicle is left with a steady state pitch angle of 3.3 degrees. The application of a control system will have two objectives during braking. Firstly, it will work to reduce the angular acceleration experienced due to the application of brakes. Secondly, it will keep the vehicle as level as possible, minimizing the steady state angle produced from the braking force.

4.4 Scenario 3 - Constant Radius Turn

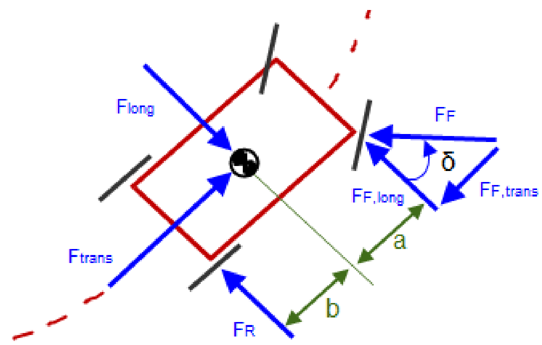

Figure 4.6: Corner Force Approximation Diagram

Unlike braking, cornering produces a moment about the roll and pitch axis. This is due to the fact that tire forces act approximately perpendicular to the plane of the tire. Figure 4.6 shows the creation of transverse forces due to the steering angle, delta.

The vehicle was simulated as completing a 0.5 g corner with a forward velocity of 22.2m/s (80km/hr). Neglecting the tire slip angles, the required steering angle, delta, can be approximated using Equation 4.4.

$$\delta = a_{LONG} * \frac{a+b}{U^2} \qquad (4.4)$$

$$\delta = 4.9\left(\frac{m}{s^2}\right) * \frac{(1.17+1.68)m}{5^2\left(\frac{m}{s^2}\right)} = 0.5586 \text{ rad}$$

The transverse and longitudinal forces, which will be applied to the pitch and roll axis of the vehicle's center of gravity were then calculated using Equation 4.5 and 4.6.

$$F_{Long} = m_{total} * a_{corner} \qquad (4.5)$$

$$F_{Long} = 1667kg * 4.9\left(\frac{m}{s^2}\right) = 8168N$$

$$F_{Trans} = \frac{F_{Long} * \sin(\delta)}{1+\cos(\delta)} \qquad (4.6)$$

$$F_{Trans} = \frac{8168\ N * \sin(0.5586)}{1 + \cos(0.5586)} = 2342N$$

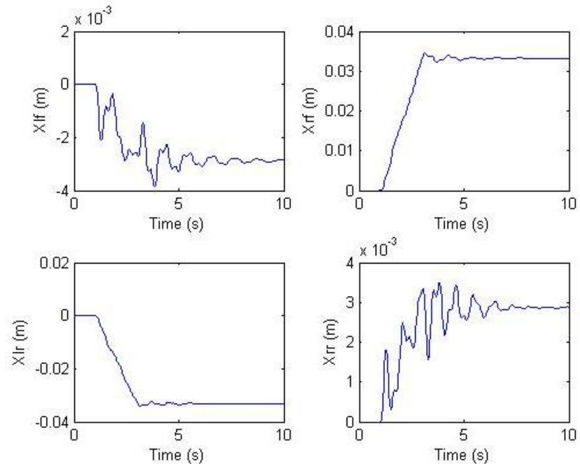

Figure 4.8: Suspension From Equilibrium, 0.5g Cornering

We simulated the vehicle with the forces discussed and produced the above plot. These data show that weight was transferred diagonally from the left rear of the vehicle, to the right front of the vehicle. This is the expected outcome of a physical vehicle which is making a left turn. It is also important to note that the suspension displacement of 3.3cm is realistic for a road going vehicle, showing that the parameter values used in Table 4.1 are reasonable. The negative value for the left rear suspension displacement represents unloading of the suspension, as a displacement of 0 m signifies the equilibrium position of the suspension system due to the vehicle sitting in a 1 g gravity field.

5. Control System Design

The objective of the control system was to reduce the roll and pitch angles of the vehicle and minimize the vertical accelerations experienced by the occupants of the vehicle. A Linear Quadratic Regulator (LQR) control strategy was selected to accomplish these goals on our Multi-Input, Multi-Output system (MIMO) linear system. The following section will detail the methodology used to implement an LQR controller.

5.1 Stability

Stability of the system was checked by determining the Eigen-values of the A matrix. All except for one of the eigen-values had a negative real component. The system's instability arose from a zero eigen-value when analyzing the open-loop dynamics. This zero eigen-value mode shape is indicative of rigid body analysis. By compressing the springs on one diagonal of the car, and extending opposing springs an equal amount, the zero eigen-value mode shape can be achieved. Releasing the system from this state will cause no chassis motion, but still allows for oscillatory motion of the suspension system. Unfortunately, this mode cannot be removed when dealing with rigid body motion, and full controllability of the system must be achieved for the implementation of an LQR controller guaranteeing stable closed loop dynamics.

5.2 Controllability

Controllability was observed by determining the rank of the controllability matrix shown as Equation 5.1 where B and A are the state space matrices as shown in Appendix C and n is the number of states; 15 for this model. It was observed that there are 9 uncontrollable states in the system using the function ctrb() in Matlab.

$$C=[B \;\; BA \;\; BA^2 \ldots\ldots\ldots\ldots BA^{n-1}\,] \qquad (5.1)$$

5.2.1 Numerical Considerations

This large quantity of uncontrollable states was surprising, and was likely the result of the matrix coefficients in the A matrix spanning more than 6 orders of magnitude. The poor conditioning of this matrix may have introduced numerical error into the "ctrb" Matlab function used to test controllability. This numerical error was confirmed by replacing every parameters shown in Table 4.1 with the value of one. Doing so greatly improved the condition of the A matrix, and when the Matlab "ctrb" function was utilized, it returned a controllability matrix of rank 1. The parameters altered were simply spring rate constants, damping constants, masses, and moments of inertia. Changing their values should have had no effect on the rank of the resulting controllability matrix. How can the numerical error due to the ill-condition of the A matrix be prevented?

Matlab functions such as modred, mineral, sminreal and balreal were utilized to attempt to correct the numerical error, but unfortunately they failed to produce a controllable system.

5.2.2 System Reduction

The full 15-state system was uncontrollable and marginally unstable which prevented successful LQR control implementation. To simplify the problem and gain controllability, the model was significantly reduced. Figure 5.1 shows the reductions made to the system bond graph. These reductions are analogues to removing the tires and un-sprung mass of the vehicle. The vehicle's suspension was now modeled as being attached directly to the road surface. The simplified model reduced the number of states from 15 to only 7.

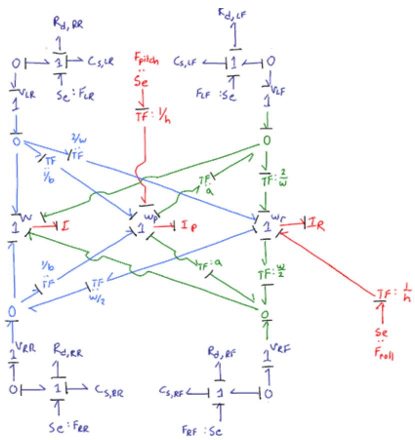

Figure 5.1: Simplified Bond Graph

Before the simplified model could be controlled, it was necessary to investigate how it performed compared to the original model. Figure 5.2 shows the original and simplified models' suspension response to the bump input discussed previously in Section 4.2. The abrupt application of the bump excited high speed oscillations in the original model due to the wheel hop natural frequency of the un-sprung mass discussed in Section 4.1. The simplified model removes the un-sprung mass as well as the tire spring, and does not exhibit high speed oscillations. The high speed oscillations are quickly damped out, leaving only the slow speed body oscillations. Both the original and simplified model exhibit similar slow speed body oscillatory motion, but the removal of the high speed dynamics from the system makes the simplified model unsuitable for controllers designed for bump disturbances.

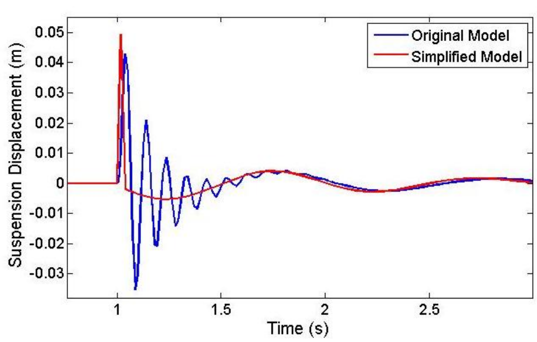

Figure 5.2: Original and Simplified Model Response to "Speed Bump"

The simplified model is however suitable for controllers designed against cornering and braking disturbances. Figure 5.3 shows the two models' response to a step input equivalent to 1g of braking force. The simplified model closely approximated the original model's dynamics. Removing the tire springs effectively removed a spring in series, which stiffened the simplified model slightly. It is no surprise that the simplified model exhibited slightly less steady state pitch when compared to the original model. The simplified model is suitable for controllers designed to encounter cornering and braking disturbances.

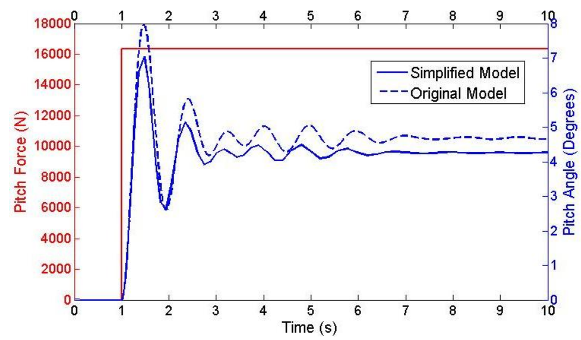

Figure 5.3: Original and Simplified Model Response to a 1g Braking Disturbance

5.2.3 Controllable Input "Trick"

Unfortunately, the reduced system had a controllability matrix with rank 6 out of 7 total states. The four force actuators situated at each corner of the vehicle were not capable of fully controlling the system. To attempt to gain controllability, the exogenous inputs were included with the controllable inputs in the formulation of the controllability matrix. The inclusion of these extra inputs produced a full rank controllability matrix, and LQR control could be designed.

It is important to note that the inclusion of inputs, which the system will have no control over, into the formulation of an LQR controller has broken the theory guaranteeing stable closed loop dynamics. The next section will detail precautions taken to minimize the risk of instability.

5.3 LQR Controller Design

The optimal state-feedback controller, Linear Quadratic Regulator was considered the best solution for the following reasons.

1. The system is modeled as Linear and it is Time Invariant (LTI).

2. The desired state does not vary with time and it is constant at equilibrium. (Regulator problem. Not a tracking problem.)
3. The need to minimize the actuator force and thus actuator power consumption.

The use of a LQR controller allowed us to achieve all our performance requirements as discussed in Section 5.3.1.

5.3.1 Design Goals

As discussed previously, the main goal of an active suspension system is to keep the vehicle as level as possible while minimizing the vertical accelerations caused due to road inputs. The passenger acceleration has been used here as an indicator of ride comfort. Therefore the effort was taken to keep the vertical acceleration within 0.98 ms^{-2}.

To quantify these abstract design goals commercial systems such as the Bose Suspension System [6] and systems discussed in reference [8] and [9] were compared. Suspension spring deflection limits were dictated by the actual mechanical limits of a suspension system in a mid-size sedan. The parameters chosen represent the maximums that a driver is expected to encounter in non-emergency situations, and a driver is unlikely to physically perceive angles less than one degree. The finalized design goals are shown in Table 5.1.

Table 5.1 : Controller Design Goals

Parameter	Value
Vehicle Pitch	1.0 deg. max.
Vehicle Roll	1.0 deg. max.
Sprung mass acceleration	0.98 ms^{-2} max.
Suspension Spring deflection	0.2 m
Settling Time	within 0.25s
Rise Time	Within 0.1s

5.3.2 State-Space Expansion

The control system design objectives discussed in Section 5.3.1 focus on the pitch and roll angles of the model. Unfortunately, the 7-state representation of the model had pitch and roll angular velocity states. To allow the controller to directly target the body angles, instead of angular velocities, the state-space representation of the model was expanded by two states, pitch angle and roll angle. Equations 5.1 and 5.2 show the two additional state equations.

$$\omega_p = \dot{\theta}_p = L_p/J_p \qquad (5.1)$$

$$\omega_r = \dot{\theta}_r = L_r/I_r \qquad (5.2)$$

5.3.3 Quadratic Cost Function

The cost function used to generate the LQR gain matrix is shown below in Equation 5.3.

$$J = \int_o^T (x^T R x + u^T \Lambda u) dt \qquad (5.3)$$

The state and input penalization matrices are shown as Equations 5.4 and 5.5.

$$R = \begin{bmatrix} 1 &&&&&&&& \\ & 1 &&&&&&& \\ && 1 &&&&&& \\ &&& 1 &&&&& \\ &&&& 1 &&&& \\ &&&&& 1 &&& \\ &&&&&& 1 && \\ &&&&&&& P & \\ &&&&&&&& R \end{bmatrix} \qquad (5.4)$$

$$\Lambda = \begin{bmatrix} 1e5 &&&&&&&&& \\ & 1e5 &&&&&&&& \\ && 1e5 &&&&&&& \\ &&& 1e5 &&&&&& \\ &&&& 1e5 &&&&& \\ &&&&& 1e5 &&&& \\ &&&&&& 1 &&& \\ &&&&&&& 1 && \\ &&&&&&&& 1 & \\ &&&&&&&&& 1 \end{bmatrix} \qquad (5.5)$$

All off diagonal terms in the state and input penalization matrices were left as zero. These terms represent penalization of combinations of different states or inputs. The first six diagonal terms of the input weighting matrix (R) penalize the use of the exogenous inputs, of which the controller has no physical control over. To minimize the use of such inputs, they were penalized by five orders of magnitude compared to the four force actuator inputs which can actually be controlled. The effects of this penalization are discussed in Section 6.1.2.

The 8th and 9th diagonal coefficients of the state weighting matrix represent the penalization of pitch angle and roll angle respectively. By changing the weighting of these coefficients compared to the other coefficients in the input and state weighting matrices, the closed loop dynamics of the system may be augmented.

Using the input and state weighting matrices, in conjunction with the open loop A and B matrices of the reduced system, a gain matrix, K, was generated using Matlab's LQR command.

5.3.4 LQR Controller Implementation

The Simulink model used to implement the gain matrix produced by the matlab LQR routine can be found in Appendix E. Disturbances are fed into the state-space block, which transforms them into outputs based on the open loop system dynamics. The outputs are then fed back into the gain matrix produced by the LQR Matlab routine. This gain matrix transforms the outputs of the system into desired inputs to control the system, which are fed back into the state-space block.

Two control architecture scenarios were studied. The first allowed for control over the four force actuators, as well as the six exogenous inputs. In reality, the controller would have no influence over the six exogenous inputs, and the second scenario severs this connection.

6. Controlled Results

This sections studies the effects of removing the link between the controller and the six exogenous inputs which it does not physically have control over. The pitch and roll weighting coefficients were set to the relatively large values of 1,000,000 so that the controller would work to minimize the pitch and roll angles of the car.

6.1 Scenario 1: Ten Controllable Inputs

The LQR controller was designed with a B matrix allowing for control over all ten inputs (including the 6 exogenous inputs). This section studies the effects of allowing the feedback control of all 10 inputs.

6.1.1 Identity Input Penalization Matrix

As discussed in Section 5.3.3, the input weighting matrix was designed to minimize the utilization of the 6 exogenous inputs by the LQR controller. Figures 6.1 though 6.4 show the response of the model when the input weighting matrix was left as identity. Figure 6.1 shows that the controller was able to reduce the pitch angle of the vehicle to less than 1.6x10^-4 degrees.

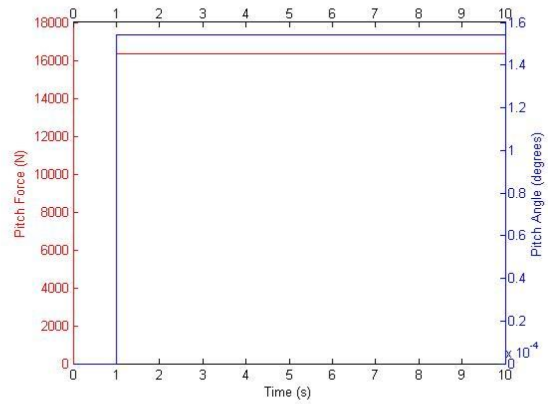

Figure 6.1: Pitch Angle Response to 1g Braking – 10 Controllable Inputs

Figure 6.2 shows force actuators had very little influence on achieving the impressively reduced roll angle, with force inputs of less than 0.01N. This is concerning, as these actuators are the only physical means that the controller has to influence the vehicle dynamics.

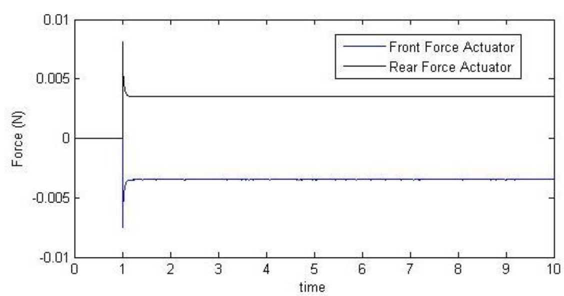

Figure 6.2: Force Actuator Response to 1g Braking – 10 Controllable Inputs

Figures 6.3 and 6.4 give insight into how the impressively small roll angle was achieved. Figure 6.3 shows that upon the application of the braking step input, the controller has requested spikes of the front and read velocity inputs. Integrated over time, these spikes correspond with changing the vertical position of the front and rear ground where the vehicle is attached. Figure 6.4 shows that the controller has changes the vertical position of the ground to effectively compress, and extend the front and rear vehicle suspension respectively. These spring displacements resist the roll angle caused by the braking step input, and the vehicle remains essentially level. Although the controller has effectively limited the vehicle's roll, it has done so using inputs to which it has no physical control.

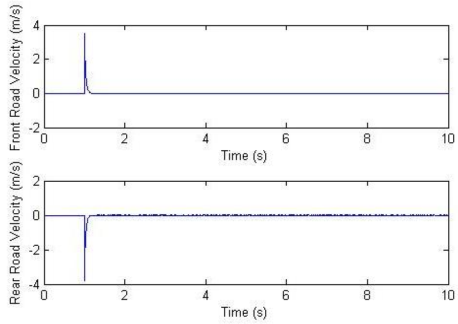

Figure 6.3: Ground Velocity Input Response to 1g Braking – 10 Controllable Inputs

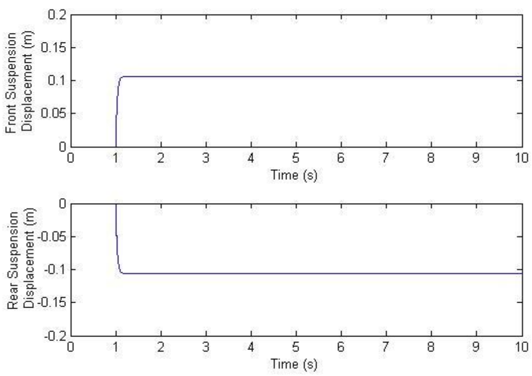

Figure 6.4: Suspension Displacement Response to 1g Braking – 10 Controllable Inputs

6.1.2 Weighted Input Penalization Matrix

This section utilizes the input weighting matrix discussed in Section 5.3.3 which heavily penalizes the use of the six exogenous inputs for controlling the system. Figure 6.5 shows that with the updated penalization matrix the controllers performance at reducing the pitch angle of the vehicle has been slightly reduced compared to the previous scenario.

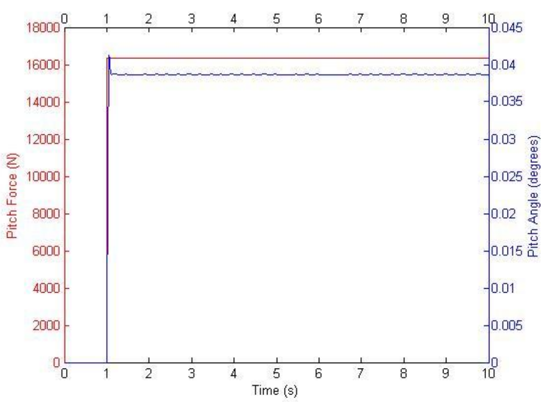

Figure 6.5: Pitch Angle Response to 1g Braking – 10 Controllable Inputs

The maximum roll angle of 0.04 degrees is however well within the design goals discussed in Section 5.3.1.

Figure 6.6 shows that the controller has began to utilize the four force actuators to limit vehicle pitch angle. Unfortunately, Figure 6.7 shows that the controller has still relied heavily on manipulating the ground velocity inputs in limiting vehicle pitch.

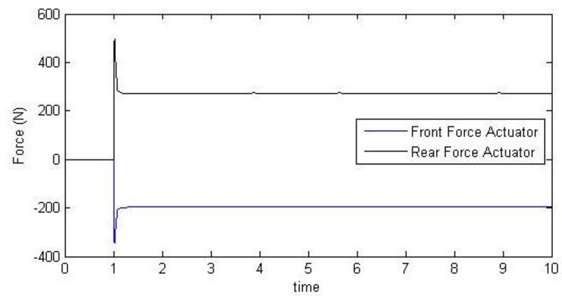

Figure 6.6: Force Actuator Input Response to 1g Braking – 10 Controllable Inputs

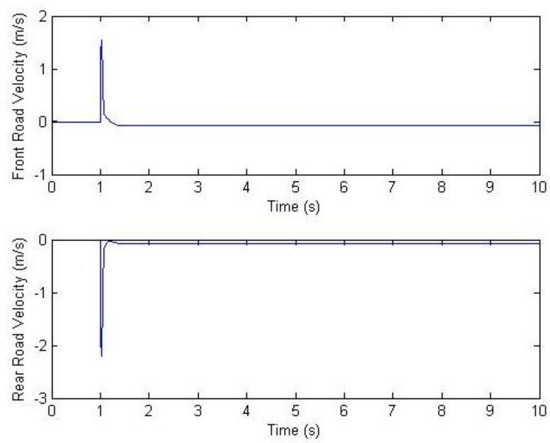

Figure 6.7: Suspension Displacement Response to 1g Braking – 10 Controllable Inputs

6.2 Scenario 2: 4 Controllable Inputs

This section discusses the ramifications of removing the link between the controller, and the 6 exogenous inputs. To accomplish this, the bond highlighted in red in the Simulink model (shown in Appendix F) has been removed. When this model is executed, Matlab returns a warning, but successfully simulates the model.

6.2.1 Identity Input Penalization Matrix

With an identity input weighting matrix, the LQR controller relies heavily on the 6 exogenous inputs when designing the gain matrix used to control the system. Removing the feedback connection of these 6 inputs has greatly reduced the effectiveness of the controller, as seen below in Figure 6.8.

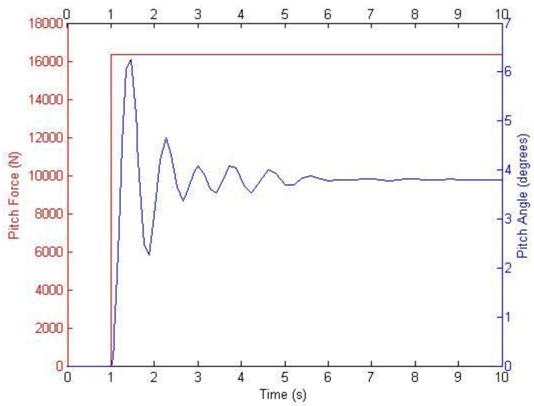

Figure 6.8: Pitch Angle Response to 1g Braking – 4 Controllable Inputs

Figure 6.9 demonstrates that the controller utilized the force actuators to attempt to limit the pitch of the vehicle. Unfortunately, the gain matrix was designed to utilize the force actuators in conjunction with the 6 exogenous inputs and did not produce forces large enough to substantially limit pitch angle.

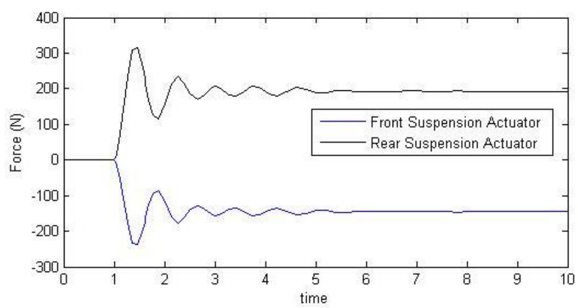

Figure 6.9: Force Actuator Input Response to 1g Braking – 4 Controllable Inputs

It is important to note that by removing the connection between the gain matrix and the 6 exogenous inputs, the LQR control theory has been violated. The closed loop system is no longer guaranteed to be stable. Fortunately the system remained stable when variations of input and state weighting matrix values were simulated.

Fear of potential instabilities led to intentional attempts to make the system unstable, or "break the controller." Many different scenarios were attempted to test the robustness of the controller. Initially, the gains in the state and input weighting matrix were modified, being made extremely large or small relative to one another. These changes did not cause the system to lose stability. Additionally, nonzero values were added to the off diagonal terms on both weighting matricides. These changes did not result in instabilities either. Overall, the controller appeared to be very robust considering the fact that the theory employed was not entirely complete.

6.2.2 Weighted Input Penalization Matrix

The input weighting matrix was again returned to the values displayed in Section5.3.3. These values penalized the use of the exogenous inputs, favoring the use of the four controllable force actuators. As compared to the results discussed in Section 6.1.2, only the four controllable actuator inputs were fed back to control the system.

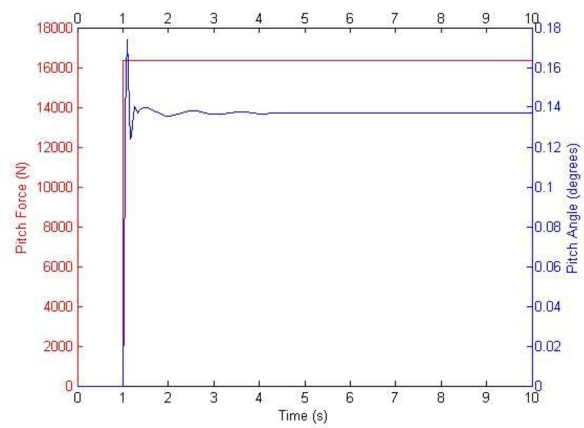

Figure 6.10: Pitch Angle Response to 1g Braking – 4 Controllable Inputs

Figure 6.10 shows that this control architecture was able to greatly reduce the pitch angle observed due a 1g braking step input. This reduction in pitch angle was achieved solely utilizing the four force actuator inputs, shown in Figure 6.11. This control configuration was selected for optimization in the next section due to its ability to adequately control the dynamics of the vehicle's chassis utilizing only the four controllable force actuators.

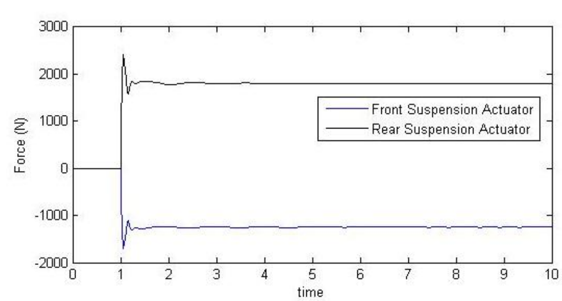

Figure 6.11: Force Actuator Input Response to 1g Braking – 4 Controllable Inputs

6.3 Controller Optimization

6.3.1 Pitch Optimization

Scenario 2 (Section 6.2) proved to be more realistic then Scenario 1 (Section 6.1), and was selected for controller optimization. Figure 6.12 shows the effect of the pitch weighting coefficient discussed in Section 5.3.3. The uncontrolled system exhibited a maximum pitch angle of 8degrees and a steady state pitch angle of almost 5 degrees. Increasing the penalization of pitch angle in the state weight matrix greatly reduced the resulting maximum and steady state pitch angles.

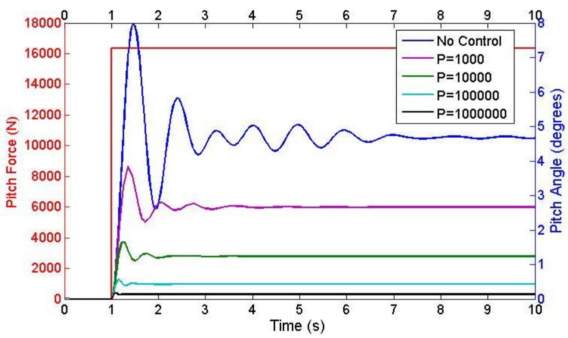

Figure 6.12: Pitch Angle Optimization – 1g Braking Step Input

Figure 6.13 shows the actuator forces at one corner of the vehicle, produced by increasing pitch angle penalization. It is clear that increased penalization of pitch angle increased the force, and thus power demanded from the actuator system. As control system designers it was our responsibility to select “P” to satisfy our design objectives, while minimizing the required actuator forces. The pitch penalization coefficient of 100,000 was selected as it bounded the pitch angle to less than the design specification of 1degree during the maximum anticipated braking of 1g while utilizing the least actuator force.

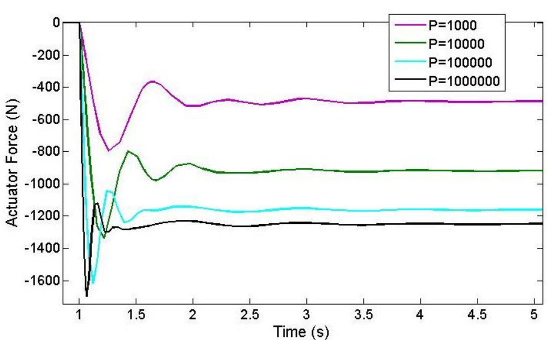

Figure 6.13: Actuator Force Required for Differing Pitch Penalization Coefficients

6.3.2 Roll Optimization

Similarly to the previous section, the controller’s sensitivity to the pitch penalizing coefficient discussed in Section 5.3.3 was studied. Figure 6.14 compares the roll angle the vehicle assumed as a result of a step input roll force equivalent to cornering at 0.5g. With no control system, the vehicle exhibited a maximum roll angle of 12 degrees, and a steady state roll angle of more than 7 degrees. Implementing an LQR derived control system with a roll penalization coefficient of 1000 moderately improved the performance of the vehicle. Increasing the value of the roll penalization coefficient significantly reduced the maximum and steady state roll angles of the vehicle to less than 1 degree.

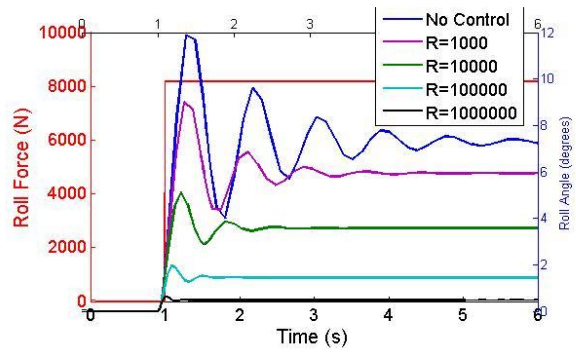

Figure 6.14: Roll Angle Optimization – 0.5g Cornering Roll Step Input

Increasing the penalization of the roll angle reduced the vehicle roll. This however occurred at the cost of increased force required by the four suspension force actuators. This is shown in Figure 6.15. To limit vehicle roll to less than the design specification of 1degree the maximum roll penalization value of 1,000,000 was required. This value was used for the optimized control system discussed in the next section.

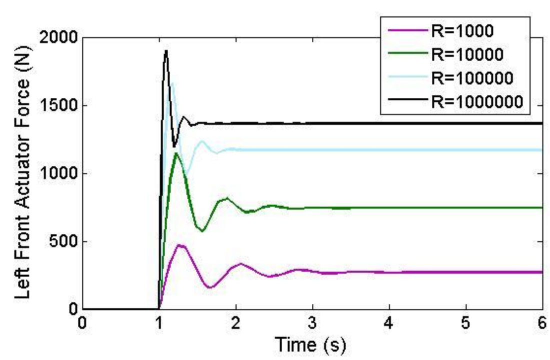

Figure 6.15: Actuator Force Required for Differing Roll Penalization Coefficients

7. Optimum Controller

The optimum controller was selected with input and state weighting matrices shown in Section 5.3.3. The vehicle was simulated cornering at 0.5g, which produced a rolling force of 8168N and a pitching force of 2342N as discussed in Section 4.4. Figures 7.1 and 7.2 show that the controller has limited vehicle pitch and roll to well within the design specifications discussed in Section 5.3.1.

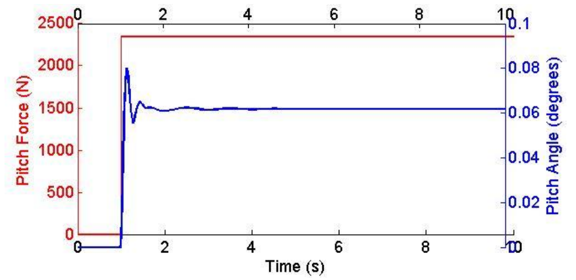

Figure 7.1: Optimum Vehicle Pitch Force and Angle Response

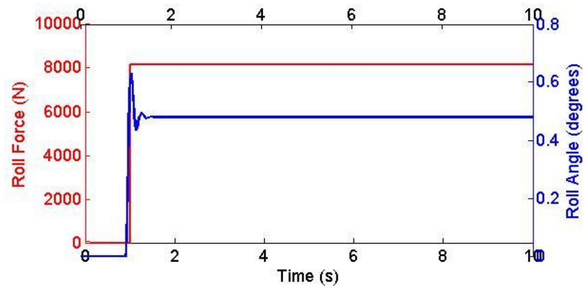

Figure 7.2: Optimum Vehicle Roll Force and Angle Response

The required actuator forces from each corner of the vehicle are shown below in Figure 7.3. As expected, the right front and left rear actuators are required to supply a larger amount of force due to the diagonal weight transfer phenomenon discussed in Section 4.4.

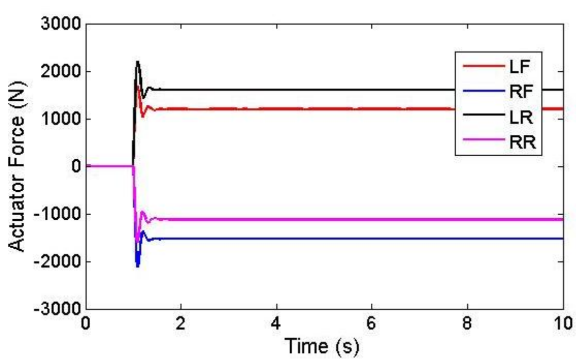

Figure 7.3: Optimum Actuator Force Responses

Unfortunately, the limitation of the non-linear tire model discussed in Section 3.2 may have been exceeded. Figure 7.3 displays the left rear force actuator exerting a tension force of 2000N. This tension force can be no larger than the corner weight of the vehicle, or else the physical tire may lift off of the ground. Based on the parameters discussed in 4.1, 41% of the 1513kg vehicle mass is statically situated over the rear axle. This is equivalent to a static mass of 310.6kg equating to 3047N of force applied statically to the left rear corner of the vehicle due to gravity. This means that the left rear force actuator may request no more than 3047N of tensile force from the static vehicle, or else the tire will lift off the ground.

Unfortunately, the dynamic vehicle assumes a different weight distribution then the static vehicle. Further investigation is necessary to ensure that the linear tire model is not operated in its unrealistic region detailed in Figure 4.1. This analysis is complicated by the removal of the tire model, and tire deflection states when the model was simplified.

If it was determined that the tires were at risk of being operating outside of their linearly acceptable region, a more complicated control system may be required. This system would need to sense the approach of tire lifting, and change its control algorithms to avoid such a phenomenon. Such a control system was deemed outside the scope of this project.

8. Conclusions

A linear vehicle dynamics model has been constructed which focuses on the vertical motion of a vehicle due to road irregularities. This model avoids the use of complicated lateral/longitudinal vehicle dynamics, and instead approximated their application to the CG of the vehicle.

The model has been validated in quarter car, and full car simulations. The model successfully approximated bump, brake, and cornering situations.

Future work will be to improve passenger ride comfort by implementing an active suspension control system. This improvement will be accomplished through the utilization of force actuators tied into each corner of the vehicle's suspension system.

6. References

[1] Bose Corporation. *The Bose Suspension System* (2004). http://www.bose.com/pdf/technologies/bose_suspension_system.pdf)

[2] Shim, Taehyun, Magolis, Donald (2001). "A bond graph model incorporating sensors, actuators, and vehicle dynamics for developing controllers for vehicle safety," *Journal of the Franklin Institute 338 (2001)* pp.21-34

[3] Milliken, Douglas L., Milliken, William F. *Race Car Vehicle Dynamics,* SAE International (2003).

[4] Karnopp, Dean(1976). "Bond Graphs for Vehicle Dynamics," *Vehicle System Dynamics*, 5: 3, 171 — 184

[5] Karnopp, Dean C., Margolis, Donald L. Rosenberg, Ronald C. *System Dynamics – Modeling and Simulation of Mechatronic Systems.* 4th ed. New York : John Wiley (2006)

[6] Karnopp, Dean C., Margolis, Donald L. *Engineering Applications of Dynamics*. New York : John Wiley (2007)

[7] Sam, Y.M., Ghani, M.R.H.A, Ahmad, N. (2000). "LQR controller for active car suspension" *TENCON 2000 Proceedings* Volume 1. pp.441-444

[8] Hrovat, D., "Applications of Optimal Control to Advanced Automotive Suspension Design," J. of Dynamic Systems, Measurement, and Control, Vol. 115, No.2(B), June 1993, pp.328-342.

[9] Zhang, B. Fan M, Miao F., "Optimal Control of Vehicle Active Suspension Systems with Actuator Delay," 2007 IEEE International Conference on Control and Automation, Guangzhou, CHINA - June 2007.

Appendix List

A : 1. Full Bond Graphs

2. Simplified Bond Graph

B : State Equations

C : 1. State Space Representation : A, B, C, D matrices

2. Modified State Space Representation

D : Complete Simulink Model

E : Complete Simulink Model with LQR

F: Modified Simulink model with LQR

G: MATLAB code

Appendix A.1 : Full Bond Graph

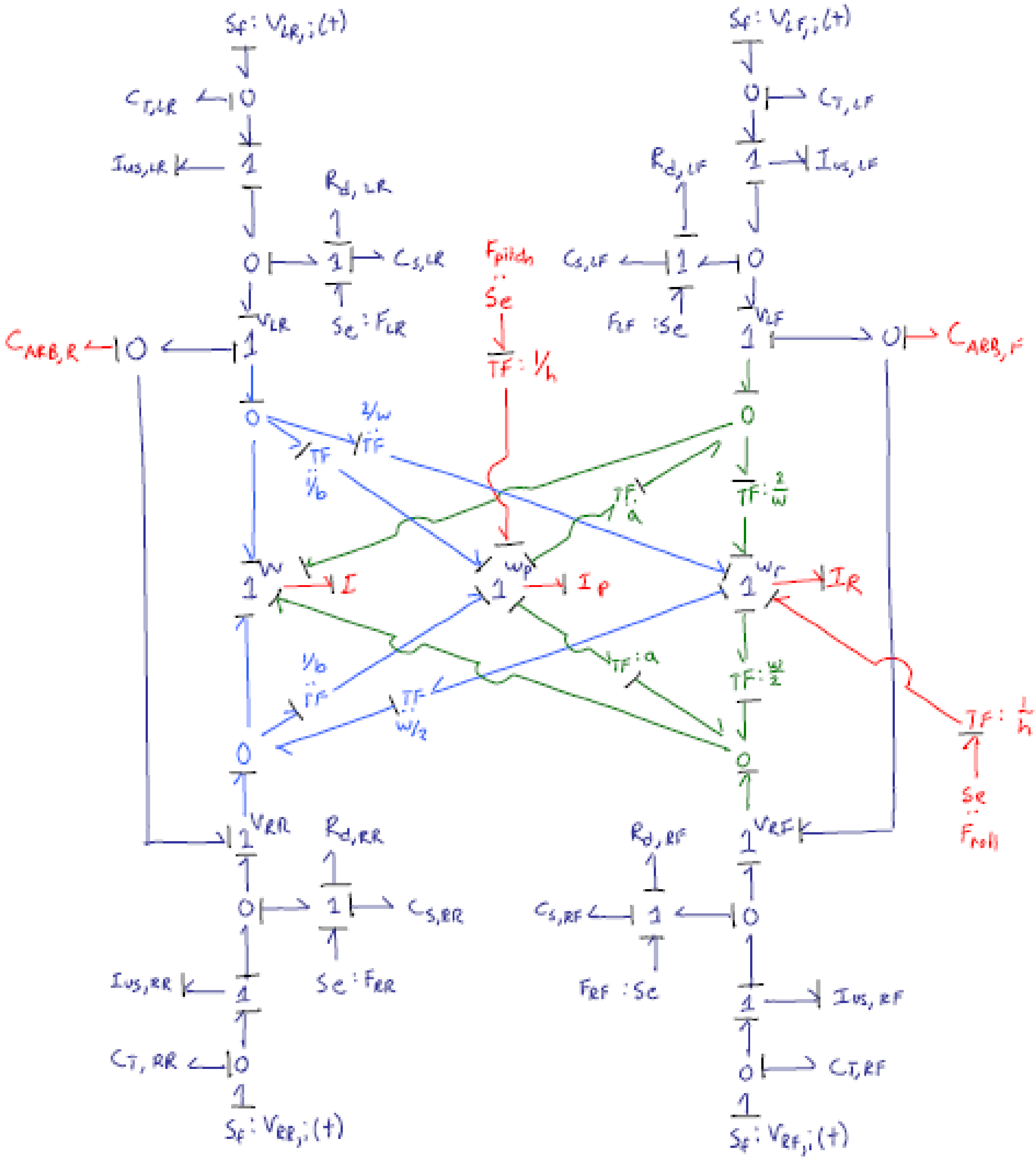

Appendix A.2 : Simplified Bond Graph

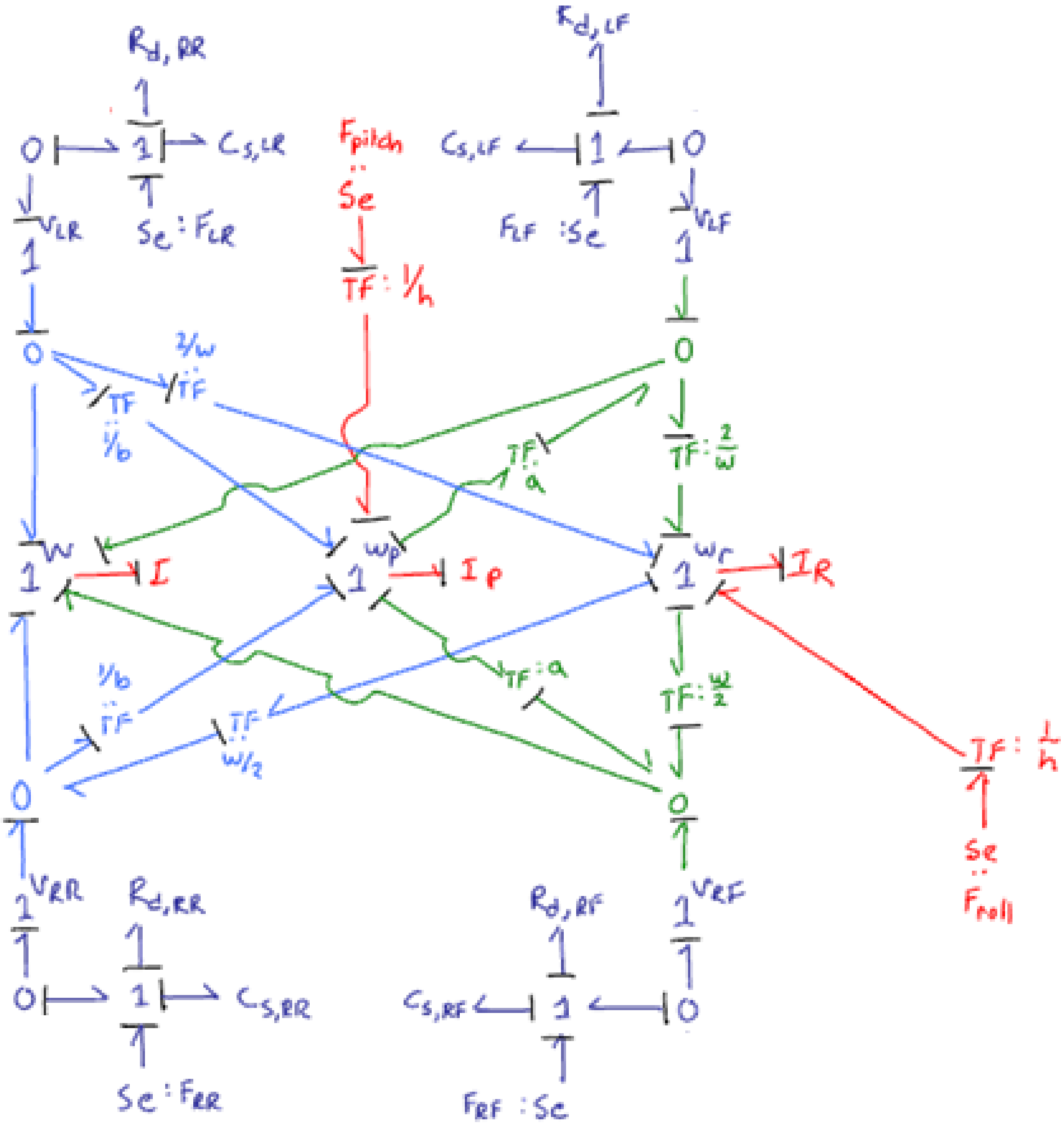

Appendix B: State Equations

Tire Springs

$$\dot{x}_{TRR} = V_{RR(t)} - \frac{p_{usRR}}{m_{us}}$$

$$\dot{x}_{TRL} = V_{RL(t)} - \frac{p_{usRL}}{m_{us}}$$

$$\dot{x}_{TFR} = V_{FL(t)} - \frac{p_{usFR}}{m_{us}}$$

$$\dot{x}_{TFL} = V_{FR(t)} - \frac{p_{usFL}}{m_{us}}$$

Anti-roll bars

$$\dot{x}_{RBR} = w\left(\frac{L_R}{J_r}\right)$$

$$\dot{x}_{RBF} = w\left(\frac{L_R}{J_r}\right)$$

Unsprung mass momentum

$$\dot{p}_{usRR} = \frac{x_{TRR}}{k_t} - \left[-F_{RR} - \frac{x_{SRR}}{k_s} + b_{sR}\left[\frac{p_{usRR}}{m_{us}} - \frac{p_{VCG}}{m_s} - b\left(\frac{L_P}{J_p}\right) + \frac{w}{2}\left(\frac{L_R}{J_r}\right)\right]\right]$$

$$\dot{p}_{usRL} = \frac{x_{TRL}}{k_t} - \left[-F_{RL} - \frac{x_{SRL}}{k_s} + b_{sR}\left[\frac{p_{usRL}}{m_{us}} - \frac{p_{VCG}}{m_s} - b\left(\frac{L_P}{J_p}\right) - \frac{w}{2}\left(\frac{L_R}{J_r}\right)\right]\right]$$

$$\dot{p}_{usFR} = \frac{x_{TFR}}{k_t} - \left[-F_{FR} - \frac{x_{SFR}}{k_s} + b_{sF}\left[\frac{p_{usFR}}{m_{us}} - \frac{p_{VCG}}{m_s} + a\left(\frac{L_P}{J_p}\right) + \frac{w}{2}\left(\frac{L_R}{J_r}\right)\right]\right]$$

$$\dot{p}_{usFL} = \frac{x_{TFL}}{k_t} - \left[-F_{FL} - \frac{x_{SFL}}{k_s} + b_{sF}\left[\frac{p_{usFL}}{m_{us}} - \frac{p_{VCG}}{m_s} + a\left(\frac{L_P}{J_p}\right) - \frac{w}{2}\left(\frac{L_R}{J_r}\right)\right]\right]$$

Rate of suspension spring deflections

$$\dot{x}_{SRR} = \frac{p_{usRR}}{m_{us}} - \left[\frac{p_{VCG}}{m_s} + b\left(\frac{L_P}{J_p}\right) - \frac{w}{2}\left(\frac{L_R}{J_r}\right)\right]$$

$$\dot{x}_{SRL} = \frac{p_{usRL}}{m_{us}} - \left[\frac{p_{VCG}}{m_s} - a\left(\frac{L_P}{J_p}\right) + \frac{w}{2}\left(\frac{L_R}{J_r}\right)\right]$$

$$\dot{x}_{SFR} = \frac{p_{usFR}}{m_{us}} - \left[\frac{p_{VCG}}{m_s} + b\left(\frac{L_P}{J_p}\right) + \frac{w}{2}\left(\frac{L_R}{J_r}\right)\right]$$

$$\dot{x}_{SFL} = \frac{p_{usFL}}{m_{us}} - \left[\frac{p_{VCG}}{m_s} - a\left(\frac{L_P}{J_p}\right) + \frac{w}{2}\left(\frac{L_R}{J_r}\right)\right]$$

Vertical Momentum of Cg

$$\begin{aligned}\dot{p}_{VCG} = {} & -F_{FR} - \frac{x_{SFR}}{k_s} + b_{sF}\left[\frac{p_{usFL}}{m_{us}} - \frac{p_{VCG}}{m_s} + a\left(\frac{L_P}{J_p}\right) + \frac{w}{2}\left(\frac{L_R}{J_r}\right)\right] - F_{RR} + \frac{x_{SRR}}{k_s} \\ & + b_{sF}\left[\frac{p_{usRR}}{m_{us}} - \frac{p_{VCG}}{m_s} - b\left(\frac{L_P}{J_p}\right) + \frac{w}{2}\left(\frac{L_R}{J_r}\right)\right] - F_{RL} + \frac{x_{SRL}}{k_s} \\ & + b_{sR}\left[\frac{p_{usRL}}{m_{us}} - \frac{p_{VCG}}{m_s} - b\left(\frac{L_P}{J_p}\right) - \frac{w}{2}\left(\frac{L_R}{J_r}\right)\right] - F_{FL} + \frac{x_{SFL}}{k_s} \\ & + b_{sR}\left[\frac{p_{usFR}}{m_{us}} - \frac{p_{VCG}}{m_s} + a\left(\frac{L_P}{J_p}\right) - \frac{w}{2}\left(\frac{L_R}{J_r}\right)\right]\end{aligned}$$

$$\begin{aligned}\dot{L}_p = {} & h\left(F_{pitc\,h}\right) + a\left[-\frac{x_{RBF}}{K_{RF}} + F_{FR} - \frac{x_{SFR}}{k_s} - b_{sF}\left[\frac{p_{usFR}}{m_{us}} - \frac{p_{VCG}}{m_s} + a\left(\frac{L_P}{J_p}\right) + \frac{w}{2}\left(\frac{L_R}{J_r}\right)\right]\right] \\ & + a\left[\frac{x_{RBF}}{K_{RF}} + F_{FL} - \frac{x_{SFL}}{k_s} - b_{sR}\left[\frac{p_{usFL}}{m_{us}} - \frac{p_{VCG}}{m_s} + a\left(\frac{L_P}{J_p}\right) - \frac{w}{2}\left(\frac{L_R}{J_r}\right)\right]\right] \\ & + b\left[\frac{x_{RBR}}{K_{RR}} - F_{RR} + \frac{x_{SRR}}{k_s} + b_{sF}\left[\frac{p_{usRR}}{m_{us}} - \frac{p_{VCG}}{m_s} - b\left(\frac{L_P}{J_p}\right) + \frac{w}{2}\left(\frac{L_R}{J_r}\right)\right]\right] \\ & + b\left[-\frac{x_{RBR}}{K_{RR}} - F_{RL} - \frac{x_{SRL}}{k_s} + b_{sR}\left[\frac{p_{usRL}}{m_{us}} - \frac{p_{VCG}}{m_s} - b\left(\frac{L_P}{J_p}\right) - \frac{w}{2}\left(\frac{L_R}{J_r}\right)\right]\right]\end{aligned}$$

$$\dot{L}_R = h(F_{roll}) - \frac{w}{2}\left[\frac{x_{RBR}}{K_{RF}} - F_{FR} + \frac{x_{SFR}}{k_s} + b_{sF}\left[\frac{p_{57}}{m_{us}} - \frac{p_{VCG}}{m_s} + a\left(\frac{L_P}{J_p}\right) + \frac{w}{2}\left(\frac{L_R}{J_r}\right)\right]\right]$$
$$- \frac{w}{2}\left[\frac{x_{RBR}}{K_{RF}} + F_{FL} - \frac{x_{SFL}}{k_s} - b_{sF}\left[\frac{p_{32}}{m_{us}} - \frac{p_{VCG}}{m_s} + a\left(\frac{L_P}{J_p}\right) - \frac{w}{2}\left(\frac{L_R}{J_r}\right)\right]\right]$$
$$- \frac{w}{2}\left[\frac{x_{RBF}}{K_{RR}} - F_{RR} + \frac{x_{SRR}}{k_s} + b_{sR}\left[\frac{p_{usRR}}{m_{us}} - \frac{p_{VCG}}{m_s} - b\left(\frac{L_P}{J_p}\right) + \frac{w}{2}\left(\frac{L_R}{J_r}\right)\right]\right]$$
$$- \frac{w}{2}\left[-\frac{x_{RBF}}{K_{RR}} - F_{RL} - \frac{x_{SRL}}{k_s} + b_{sR}\left[\frac{p_{usRL}}{m_{us}} - \frac{p_{VCG}}{m_s} - b\left(\frac{L_P}{J_p}\right) - \frac{w}{2}\left(\frac{L_R}{J_r}\right)\right]\right]$$

Appendix C.1 : Original State Space Representation
States X, Inputs U and A, B, C, D matrices

$$
X = \begin{bmatrix} x_{TRL} \\ x_{TFR} \\ x_{SRL} \\ x_{TFL} \\ x_{TRR} \\ x_{SFR} \\ x_{RBR} \\ x_{SFL} \\ p_{usRL} \\ x_{SRR} \\ p_{usFR} \\ x_{RBR} \\ p_{usFL} \\ p_{usRR} \\ L_R \\ L_P \\ p_{VCG} \end{bmatrix}
\qquad
U = \begin{bmatrix} V_{RR} \\ F_{RR} \\ F_{LR} \\ V_{RL} \\ V_{FL} \\ F_{FL} \\ F_{roll} \\ F_{FR} \\ V_{FR} \\ F_{pitch} \end{bmatrix}
\qquad
B = \begin{bmatrix}
0 & 0 & 0 & 1 & 0 & 0 & 0 & 0 & 0 & 0 \\
0 & 0 & 0 & 0 & 0 & 0 & 0 & 0 & 1 & 0 \\
0 & 0 & 0 & 0 & 0 & 0 & 0 & 0 & 0 & 0 \\
0 & 0 & 0 & 0 & 1 & 0 & 0 & 0 & 0 & 0 \\
0 & 0 & 0 & 0 & 0 & 0 & 0 & 0 & 0 & 0 \\
0 & 0 & 0 & 0 & 0 & 0 & 0 & 0 & 0 & 0 \\
0 & 0 & 0 & 0 & 0 & 0 & 0 & 0 & 0 & 0 \\
0 & 0 & 0 & 0 & 0 & 0 & 0 & 0 & 0 & 0 \\
0 & 0 & 1 & 0 & 0 & 0 & 0 & 0 & 0 & 0 \\
0 & 0 & 0 & 0 & 0 & 0 & 0 & 0 & 0 & 0 \\
0 & 1 & 0 & 0 & 0 & 0 & 0 & 0 & 0 & 0 \\
0 & 0 & 0 & 0 & 0 & 1 & 0 & 0 & 0 & 0 \\
1 & 0 & 0 & 0 & 0 & 0 & 0 & 0 & 0 & 0 \\
0 & 0 & 0 & 0 & 0 & 0 & 1 & 0 & 0 & 0 \\
0 & 0 & 0 & 0 & 0 & 0 & 0 & 1 & 0 & 0 \\
0 & 0 & 1 & 0 & 0 & 0 & 1 & 0 & 0 & 0 \\
1 & 0 & 0 & 0 & 0 & 0 & 0 & 0 & 1 & 0
\end{bmatrix}
\qquad
D_{(7x17)} = 0
$$

$$
A = \begin{bmatrix}
0 & 0 & 0 & 0 & 0 & 0 & 0 & 0 & \frac{-1}{m_{us}} & 0 & 0 & 0 & 0 & 0 & 0 & 0 & 0 \\
0 & 0 & 0 & 0 & 0 & 0 & 0 & 0 & 0 & 0 & \frac{-1}{m_{us}} & 0 & 0 & 0 & 0 & 0 & 0 \\
0 & 0 & 0 & 0 & 0 & 0 & 0 & 0 & \frac{1}{m_{us}} & 0 & 0 & 0 & 0 & 0 & -w/(2*J_r) & \frac{-b}{J_r} & \frac{-1}{m_s} \\
0 & 0 & 0 & 0 & 0 & 0 & 0 & 0 & 0 & 0 & 0 & 0 & \frac{-1}{m_{us}} & 0 & 0 & 0 & 0 \\
0 & 0 & 0 & 0 & 0 & 0 & 0 & 0 & 0 & 0 & 0 & 0 & 0 & \frac{-1}{m_{us}} & 0 & 0 & 0 \\
0 & 0 & 0 & 0 & 0 & 0 & 0 & 0 & 0 & 0 & \frac{1}{m_{us}} & 0 & 0 & 0 & -w/(2*J_r) & \frac{a}{J_p} & \frac{1}{m_s} \\
0 & 0 & 0 & 0 & 0 & 0 & 0 & 0 & 0 & 0 & 0 & 0 & 0 & 0 & (\frac{w}{2})/(J_r+J_r) & 0 & 0 \\
0 & 0 & 0 & 0 & 0 & 0 & 0 & 0 & 0 & 0 & 0 & 0 & \frac{1}{m_{us}} & -w/(2*J_r) & \frac{a}{J_p} & 0 & 0 \\
 & & & & & & & & & & \ldots\ldots\ldots. & & & & & & \\
 & & & & & & & & & & Etc. & & & & & & \\
 & & & & & & & & & & \ldots\ldots\ldots & & & & & &
\end{bmatrix}
$$

Please refer to the MATLAB code in Appendix E for the complete A matrix programmed in.

$$
C = \begin{bmatrix}
0 & 0 & \mathbf{1} & 0 & 0 & 0 & 0 & 0 & 0 & 0 & 0 & 0 & 0 & 0 & 0 & 0 & 0 \\
0 & 0 & 0 & 0 & 0 & 0 & 0 & \mathbf{1} & 0 & 0 & 0 & 0 & 0 & 0 & 0 & 0 & 0 \\
0 & 0 & 0 & 0 & 0 & \mathbf{1} & 0 & 0 & 0 & 0 & 0 & 0 & 0 & 0 & 0 & 0 & 0 \\
0 & 0 & 0 & 0 & 0 & 0 & 0 & 0 & 0 & \mathbf{1} & 0 & 0 & 0 & 0 & 0 & 0 & 0 \\
0 & 0 & 0 & 0 & 0 & 0 & 0 & 0 & 0 & 0 & 0 & 0 & 0 & 0 & 0 & 0 & 1/m_s \\
0 & 0 & 0 & 0 & 0 & 0 & 0 & 0 & 0 & 0 & 0 & 0 & 0 & 0 & 0 & 1/J_p & 0 \\
0 & 0 & 0 & 0 & 0 & 0 & 0 & 0 & 0 & 0 & 0 & 0 & 0 & 0 & 1/J_r & 0 & 0
\end{bmatrix}
$$

Appendix C.2 : Modified State Space Representation
States X, Inputs U and A, B, C, D matrices

$$X = \begin{bmatrix} x_{SRL} \\ x_{SFR} \\ x_{SFL} \\ x_{SRR} \\ p_{VCG} \\ L_R \\ L_P \\ \theta_r \\ \theta_p \end{bmatrix} \qquad U = \begin{bmatrix} V_{RR} \\ F_{RR} \\ F_{LR} \\ V_{RL} \\ V_{FL} \\ F_{FL} \\ F_{roll} \\ F_{FR} \\ V_{FR} \\ F_{pitc\,h} \end{bmatrix} \qquad B = \begin{bmatrix} 0 & 0 & 0 & 1 & 0 & 0 & 0 & 0 & 0 & 0 \\ 0 & 0 & 0 & 0 & 0 & 0 & 0 & 0 & 1 & 0 \\ 0 & 0 & 0 & 0 & 0 & 0 & 0 & 0 & 0 & 0 \\ 0 & 0 & 0 & 0 & 1 & 0 & 0 & 0 & 0 & 0 \\ 0 & 0 & 0 & 0 & 0 & 0 & 0 & 0 & 0 & 0 \\ 0 & 0 & 0 & 0 & 0 & 0 & 0 & 0 & 0 & 0 \\ 0 & 0 & 0 & 0 & 0 & 0 & 0 & 0 & 0 & 0 \\ 0 & 0 & 0 & 0 & 0 & 0 & 0 & 0 & 0 & 0 \\ 0 & 0 & 1 & 0 & 0 & 0 & 0 & 0 & 0 & 0 \\ 0 & 0 & 0 & 0 & 0 & 0 & 0 & 0 & 0 & 0 \\ 0 & 1 & 0 & 0 & 0 & 0 & 0 & 0 & 0 & 0 \\ 0 & 0 & 0 & 0 & 0 & 1 & 0 & 0 & 0 & 0 \\ 1 & 0 & 0 & 0 & 0 & 0 & 0 & 0 & 0 & 0 \\ 0 & 0 & 0 & 0 & 0 & 0 & 1 & 0 & 0 & 0 \\ 0 & 0 & 0 & 0 & 0 & 0 & 0 & 1 & 0 & 0 \\ 0 & 0 & 1 & 0 & 0 & 0 & 1 & 0 & 0 & 0 \\ 1 & 0 & 0 & 0 & 0 & 0 & 0 & 0 & 1 & 0 \end{bmatrix} \qquad D_{(7x17)} = 0$$

$$A = \begin{bmatrix} \frac{-1}{m_{us}} & 0 & 0 & 0 & 0 & 0 & 0 & 0 & 0 & 0 & 0 \\ 0 & 0 & \frac{-1}{m_{us}} & 0 & 0 & 0 & 0 & 0 & 0 & 0 & 0 \\ \frac{1}{m_{us}} & 0 & 0 & 0 & 0 & 0 & -w/(2*J_r) & \frac{-b}{J_r} & \frac{-1}{m_s} & 0 & 0 \\ 0 & 0 & 0 & 0 & \frac{-1}{m_{us}} & 0 & 0 & 0 & 0 & 0 & 0 \\ 0 & 0 & \frac{1}{m_{us}} & 0 & 0 & 0 & -w/(2*J_r) & \frac{a}{J_p} & \frac{1}{m_s} & 0 & 0 \\ 0 & 0 & 0 & 0 & 0 & 0 & (\frac{w}{2})/(J_r+J_r) & 0 & 0 & 0 & 0 \\ 0 & 0 & 0 & 0 & \frac{1}{m_{us}} & -w/(2*J_r) & \frac{a}{J_r} & 0 & 0 & 0 & 0 \\ 0 & 0 & 0 & 0 & 0 & 0 & 0 & \frac{1}{J_r} & 0 & 0 & 0 \\ 0 & 0 & 0 & 0 & 0 & 0 & 0 & 0 & \frac{1}{J_p} & 0 & 0 \end{bmatrix}$$

Please refer to the MATLAB code in Appendix E for the complete A matrix programmed in.

$$C = \begin{bmatrix} \mathbf{1} & 0 & 0 & 0 & 0 & 0 & 0 & 0 & 0 \\ 0 & 0 & 0 & \mathbf{1} & 0 & 0 & 0 & 0 & 0 \\ 0 & 0 & \mathbf{1} & 0 & 0 & 0 & 0 & 0 & 0 \\ 0 & 0 & 0 & 0 & \mathbf{1} & 0 & 0 & 0 & 0 \\ 0 & 0 & 0 & 0 & 0 & 0 & 0 & 0 & 1/m_s \\ 0 & 0 & 0 & 0 & 0 & 0 & 0 & 1/J_p & 0 \\ 0 & 0 & 0 & 0 & 0 & 0 & 1/J_r & 0 & 0 \end{bmatrix}$$

Appendix D : Complete Simulink Model of the System (without the Controller)

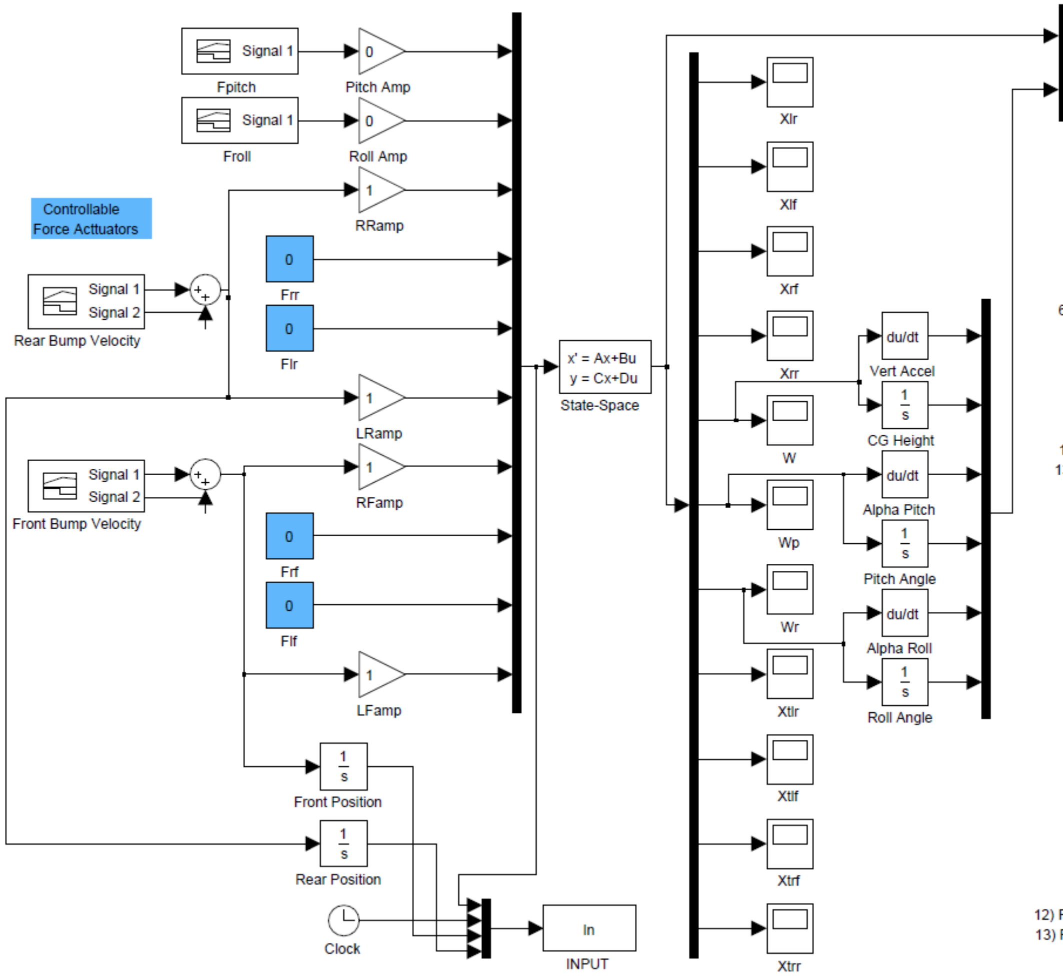

OUTPUT

Suspension Displacement:
1) LR
2) LF
3) RF
4) RR
5) CG Verticle Velocity
6) CG Pitch Angular Velocity
7) CF Roll Angular Velocity
Tire Displacement:
8) LR
9) LF
10) RF
11) RR
12) CG Verticle Acceleration
13) CG Verticle Displacement
14) CG Alpha Pitch
15) CG Pitch Angle
16) CG Alpha Roll
17) CG Roll Angle

INPUTS

1) Pitch Force
2) Roll Force
3) RR Velocity
4) RR Force Actuator
5) LR Force Actuator
6) LR Velocity
7) RF Velocity
8) RF Force Actuator
9) LF Force Actuator
10) LF Velocity
11) Time
12) Front Bump Input Position
13) Rear Bump Input Position

Appendix E : Complete Simulink Model with LQR Controller

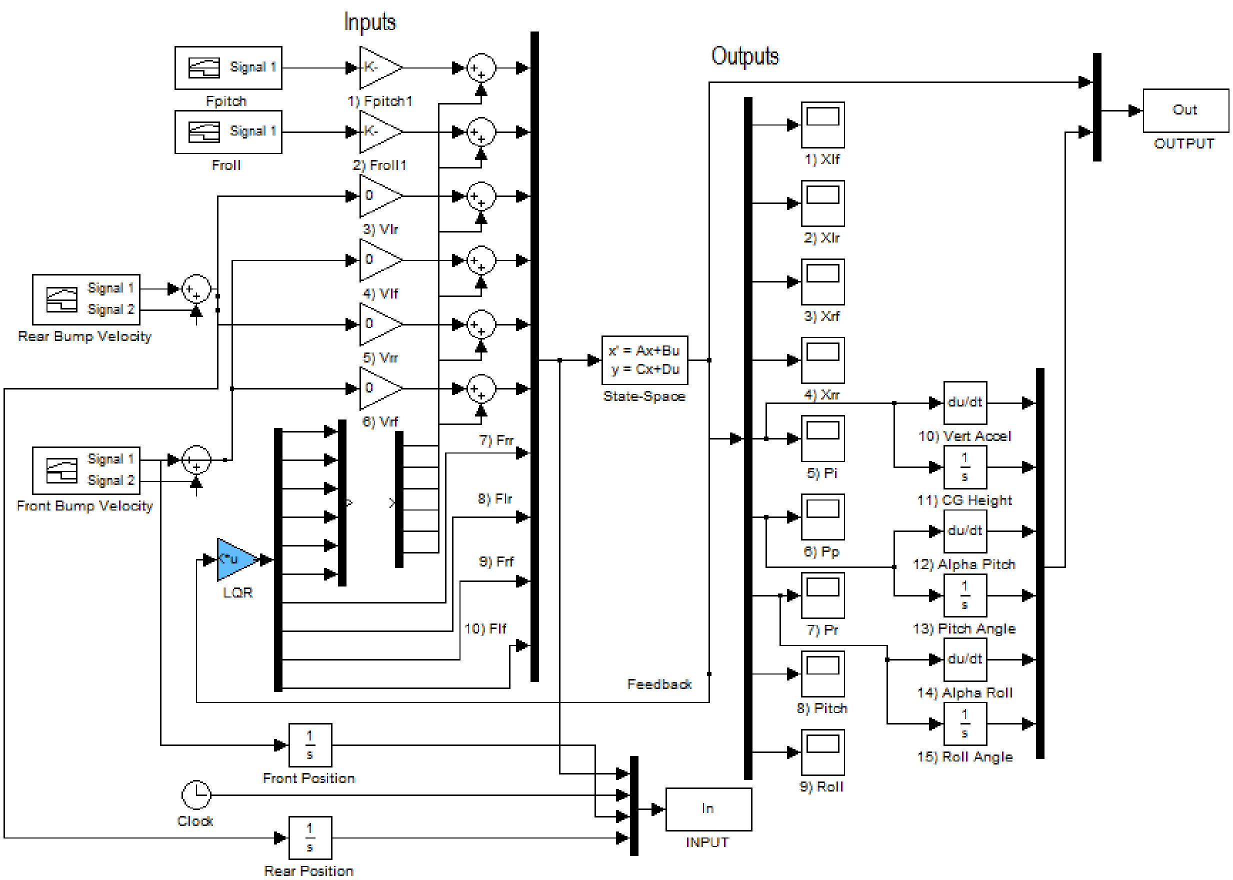

Appendix F : Modified Simulink Model with LQR

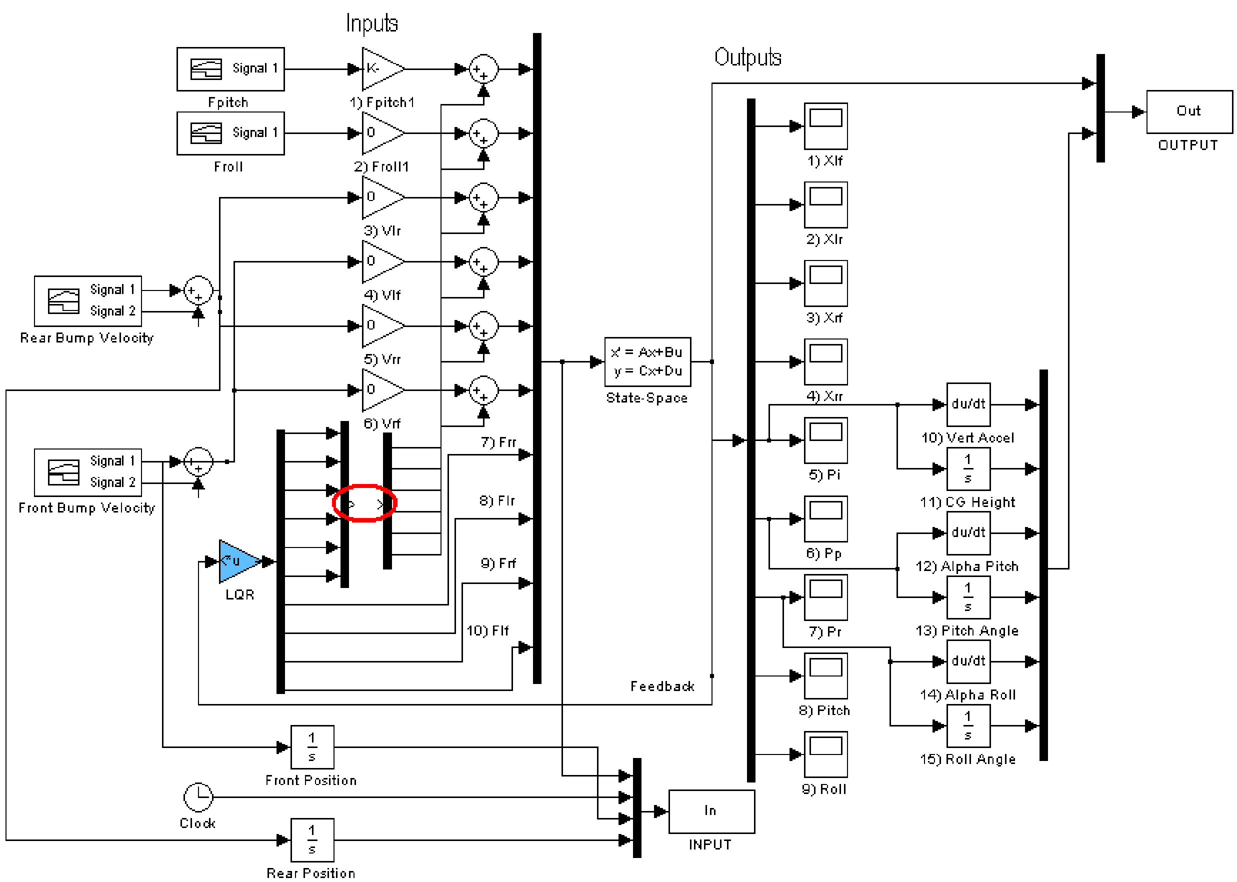

Appendix G : MATLAB code

```
%%
clear all; clc

%----State Vector------------------------------------------------------------
%... Number of States  7
% 1) Q65=Qlf;
% 2) Q38=Qlr;
% 3) Q57=Qrf;
% 4) Q28=Qrr;
% 5) P45=Pi;
% 6) P48=Pp;
% 7) P49=Pr;
% 8) Pitch Angle;
% 9) Roll Angle;
%----Geometric Parameters----------------------------------------------------
 w=1.54; %m
 h=0.55; %m
 b=1.68; %m
 a=1.17; %m

% ----Parameter Values-------------------------------------------------------
 Csrr=1/14900; %1/(N/m)
 Cslr=1/14900; %1/(N/m)
 Cslf=1/14900; %1/(N/m)
 Csrf=1/14900; %1/(N/m)

 I =1513; %kg
 Ir=637.26; %kg-m^2
 Ip=2443.26; %kg-m^2


 Rdrr=475; %N-s/m
 Rdlf=475; %N-s/m
 Rdrf=475; %N-s/m
 Rdlr=475; %N-s/m

 %----Mapping Our Variable Names to Campg Assignments----------------------
T1x2 = 2/w ;
T3x4 = 1/b ;
T5x6 = 1/b ;
T7x8 = w/2 ;
T9x10 = a ;
T11x12 = a ;
T13x14 = 1/h ;
T15x16 = 1/h ;
T17x18 = 2/w ;
T19x20 = w/2 ;
R27 = Rdrr ;
C28 = Csrr ;
R37 = Rdlr ;
C38 = Cslr ;
I45 = I ;
I48 = Ip ;
```

```
I49 = Ir ;
R56 = Rdrf ;
C57 = Csrf ;
R64 = Rdlf ;
C65 = Cslf ;

  %----Mapping Our in/out to Campg Assignments------------------------------
 % 1) SE13 = Fpitch ;
 % 2) SE15 = Froll ;
 % 3) SF21 = Vlr ;
 % 4) SF22 = Vlf ;
 % 5) SF23 = Vrr ;
 % 6) SF24 = Vrf ;
 % 7) SE29 = Frr ;
 % 8) SE39 = Flr ;
 % 9) SE58 = Frf ;
 % 10)SE66 = Flf ;


 %----Building the A and B matricies----------------------------------------
%... Number of States   7
   A(1,:) = [0,0,0,0,-1/I45,+1/I48*T9x10,-1/I49/T17x18 0 0];
   B(1,:) = [0,0,0,1,0,0,0,0,0,0];

   A(2,:) = [0,0,0,0,-1/I45,-1/I48/T3x4,-1/I49/T1x2 0 0];
   B(2,:) = [0,0,1,0,0,0,0,0,0,0];

   A(3,:) = [0,0,0,0,-1/I45,+1/I48*T11x12,+1/I49*T19x20 0 0];
   B(3,:) = [0,0,0,0,0,1,0,0,0,0];

   A(4,:) = [0,0,0,0,-1/I45,-1/I48/T5x6,+1/I49*T7x8 0 0];
   B(4,:) = [0,0,0,0,1,0,0,0,0,0];

   A(5,:) = [+1/C65,+1/C38,+1/C57,+1/C28,-1/I45*R64-1/I45*R27-1/I45*R37- ...
             1/I45*R56,+1/I48*T9x10*R64-1/I48/T5x6*R27-1/I48/T3x4*R37+ ...
            1/I48*T11x12*R56,-1/I49/T17x18*R64+1/I49*T7x8*R27-1/I49/T1x2*R37+
            ...1/I49*T19x20*R56 0 0];

   B(5,:) = [0,0,+1*R37,1*R64,+1*R27,+1*R56,-1,-1,-1,-1];

   A(6,:) = [-1/C65*T9x10,+1/C38/T3x4,-1/C57*T11x12,+1/C28/T5x6,- ...
            1/I45*R37/T3x4-1/I45*R27/T5x6+1/I45*R64*T9x10+1/I45*R56*T11x12,-
            ... 1/I48/T3x4*R37/T3x4-1/I48/T5x6*R27/T5x6-
            1/I48*T9x10*R64*T9x10- ... 1/I48*T11x12*R56*T11x12,-
            1/I49/T1x2*R37/T3x4+1/I49*T7x8*R27/T5x6+ ...
             1/I49/T17x18*R64*T9x10-1/I49*T19x20*R56*T11x12 0 0];

   B(6,:) = [+1/T13x14,0,1*R37/T3x4,-1*R64*T9x10,+1*R27/T5x6,-1*R56*T11x12,-
            1/T5x6,-1/T3x4,+1*T11x12,+1*T9x10];

   A(7,:) = [+1/C65/T17x18,+1/C38/T1x2,-1/C57*T19x20,-1/C28*T7x8,- ...
            1/I45*R37/T1x2+1/I45*R27*T7x8-
            1/I45*R64/T17x18+1/I45*R56*T19x20,- ...
```

```
            1/I48/T3x4*R37/T1x2+1/I48/T5x6*R27*T7x8+1/I48*T9x10*R64/T17x18-
            ... 1/I48*T11x12*R56*T19x20,-1/I49/T1x2*R37/T1x2-
            1/I49*T7x8*R27*T7x8- ...
             1/I49/T17x18*R64/T17x18-1/I49*T19x20*R56*T19x20 0 0];

B(7,:) = [0,+1/T15x16,1*R37/T1x2,+1*R64/T17x18,-1*R27*T7x8,-1*R56*T19x20,+
            1*T7x8,-1/T1x2,+1*T19x20,-1/T17x18];

   %Expand state space to hold pitch angle
   A(8,:) = [0 0 0 0 0 1 0 0 0];
   B(8,:) = [0 0 0 0 0 0 0 0 0 0];

   A(9,:) = [0 0 0 0 0 0 1 0 0];
   B(9,:) = [0 0 0 0 0 0 0 0 0 0];

%==========================================================================
% %Output Matrix Definition

C=eye(9);
D=zeros(9,10);

%==========================================================================
%LQR Controller Gain Design

% %state weighting
Q=eye(length(A));

%Pitch Penalty
Q(8,8)=100000;

%Roll Penalty
Q(9,9)=1000000;


%input weighting
R=eye(length(B));
R(1,1)=100000; R(2,2)=100000; R(3,3)=100000; R(4,4)=100000; R(5,5) = 100000;
R(6,6)=100000;

[K,S,e] = lqr(A,B,Q,R);
```